Electronic Supporting information:

Tailored Transition Metal-doped Nickel Phosphide Nanoparticles for Electrochemcial Oxygen Evolution Reaction (OER)

Ho-Wing Man, Chui-Shan Tsang, Molly Meng-Jung Li, Jiaying Mo, Bolong Huang, Lawrence Yoon Suk Lee, Yun-Chung Leung, Kwok-Yin Wong, and Shik Chi Edman Tsang

Experimental Details

Characterization. Powdered X-Ray diffraction pattern was obtained using Rigaku SmartLab with scan rate of 1° min^{-1}. Powdered sample was placed on a silicon wafer and pressed using a glass slide. Diffraction pattern from 2θ = 35° to 60° was obtained for pristine and various metal-doped nickel phosphide nanoparticles. As-prepared powder samples were dispersed and sonicated in chloroform to obtain well-dispersed suspension. 20-40 μL of suspension was added on a 400-mesh copper grid with holely carbon coating and dried naturally. Images from transmission electron microscopy were obtained using a scanning transmission electron microscope (JOEL JEM-2100F). Selected area electron diffraction (SAED) and energy-dispersive X-ray spectroscopy (EDX) were carried out in tandem in transmission electron microscopy. Approximately 20 mg of powder sample was used in analysis. X-Ray photoelectron spectra of pristine and various metal-doped nickel phosphide nanoparticles were obtained using X-Ray photoelectron spectrophotometer (ESCALAB 250 Xi). Calibration was done using binding energy of C 1s energy level at 284.8 eV as reference.

Preparation of working electrode. Catalyst ink was prepared by dissolving 2.5 mg metal-doped nickel phosphide nanoparticles in a solution containing 460 μL ethanol-water mixture (3:7) and 40 μL 5 wt.% Nafion solution. Working electrode was prepared by drop-casting 10 μL of catalyst ink on glassy carbon electrode (GCE, d = 3 mm, surface area = 0.0707 cm^2). The catalyst ink was dried naturally.

Measurement of performance on electrochemical OER. Electrochemical measurements were performed using a CHI potentiostat (CHI1030A). Electrocatalytic oxygen evolution reaction was conducted in a typical three-electrode system, using Pt mesh and saturated calomel electrode (SCE) as the counter and reference electrode, respectively, in 1 M potassium hydroxide solution (pH = 14). The electrolyte solution was purged with Ar for 30 min before the electrochemical measurements to get rid of dissolved oxygen and provide inert atmosphere. Linear sweep voltammetry (LSV) was carried out in a potential range of 0.13 and 0.19 V with a scan rate of 5 mV/s. The potentials measurement against saturated calomel electrode (SCE) were converted with respect to the reverse hydrogen electrode (RHE) according to the following equation:[1]

$$E_{RHE} = E_{SCE} + 0.244 + 0.0592(pH)$$

Electrochemical impedance spectroscopy. Electrochemical impedance spectroscopy (EIS) was carried out in 1 M KOH aqueous solution that was purged with Ar prior to measurement. Graphite rod and SCE were used as the counter and reference electrodes, respectively. The EIS was measured in the frequency range of 10 mHz and 1 MHz with an amplitude of 5 mV. The applied potential was 0.5 V.

Estimation of reaction order of hydroxide ion. Cyclic voltammetry was carried out from -0.1 V to 1 V *vs.* SCE under KOH solution with concentration of 0.1, 0.25, 0.5 and 1 M. Current density at 0.6 V *vs.* SCE was plotted against hydroxide ion concentration in logarithmic scale. The slope of the plot was equivalent to reaction order of hydroxide ion according to the following equation:[2]

$$m = \frac{\partial \, lnj}{\partial \, ln \, [OH^-]}$$

where m is the reaction order of hydroxide ion, and j is the current density at potential at 0.6 V *vs.* SCE.

Stability test for electrochemical OER. The working electrode coated with NiFeP nanoparticles was tested for the stability by holding the potential at 1.47 V *vs.* RHE for 4 h.

Iron-doped nickel phosphide (NiFeP) nanoparticle was first synthesized to investigate the feasibility of metal doping in nickel phosphide crystal lattice. Nickel and iron metal salts were mixed in the presence of oleylamine, trioctylphosphine (TOP), and trioctylphosphine oxide (TOPO).

X-Ray diffraction (XRD) pattern of NiFeP nanoparticles is shown below (Figure S1). The as-synthesized NiFeP nanoparticle has almost identical diffraction pattern as hcp phase of Ni_2P which consist four peaks at 2θ = 40.7°, 44.7°, 47.4°, and 54.4°. Thus, this diffraction pattern resembles closely to Ni_2P hexagonal crystal structure (PDF#-65-1989) without much peak distortion or peak shift at the high level of Fe doping although line broadening due to small sizes may have prevented accurate peaks comparison. The former three peaks from XRD pattern of NiFeP at 2θ = 40.7°, 44.7°, and 47.4° are corresponding to (111), (201), and (210) lattice planes, respectively. Meanwhile, the two peaks at 54.2° and 55° in Ni_2P reference pattern, corresponding to (300) and (211) lattice planes, respectively, merge together to have a broad peak at 54.4° in XRD pattern of NiFeP nanoparticle due to small crystalline size in nanoparticles.

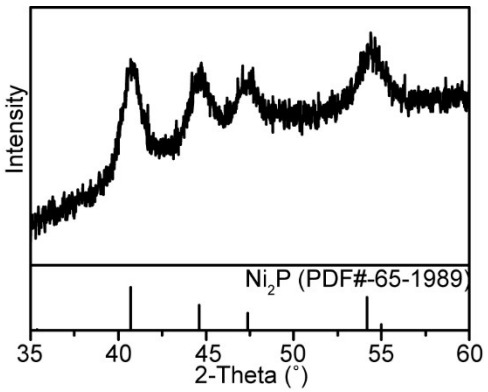

Figure S1. XRD pattern of NiFeP nanoparticle.

Detailed morphology and elemental composition of NiFeP nanoparticle are investigated by transmission electron microscopy (TEM) and energy dispersive X-ray spectroscopy (EDX) equipped in TEM. The TEM image shows the as-synthesized NiFeP nanoparticle is monodispersed and spherical with an average diameter of 7.5 ± 0.9 nm (Figure S2 (a) and (b)). The small size of nanoparticle is coherent with the large full width at half maximum (broad peaks) and small crystalline size in XRD pattern. TEM image taken under high resolution is shown in Figure S2 (c). The predominant (111) lattice fringe shows a *d*-spacing of 0.22 nm. The selected area electron diffraction (SAED) pattern shows the rings of diffraction (Figure S2 (d)), where the innermost ring is indexed as (111) lattice plane and the outermost ring corresponds to (300) lattice plane. The measurement of *d*-spacing and electron diffraction pattern is in good agreements with XRD pattern mentioned previously. The elemental composition is determined by EDX (Figure S3). The normalized ratio of elements in NiFeP nanoparticle (nickel-to-iron-to-phosphorus) is 1:0.1:0.7. An overall 6% of iron is successfully doped into the nickel phosphide crystal lattice.

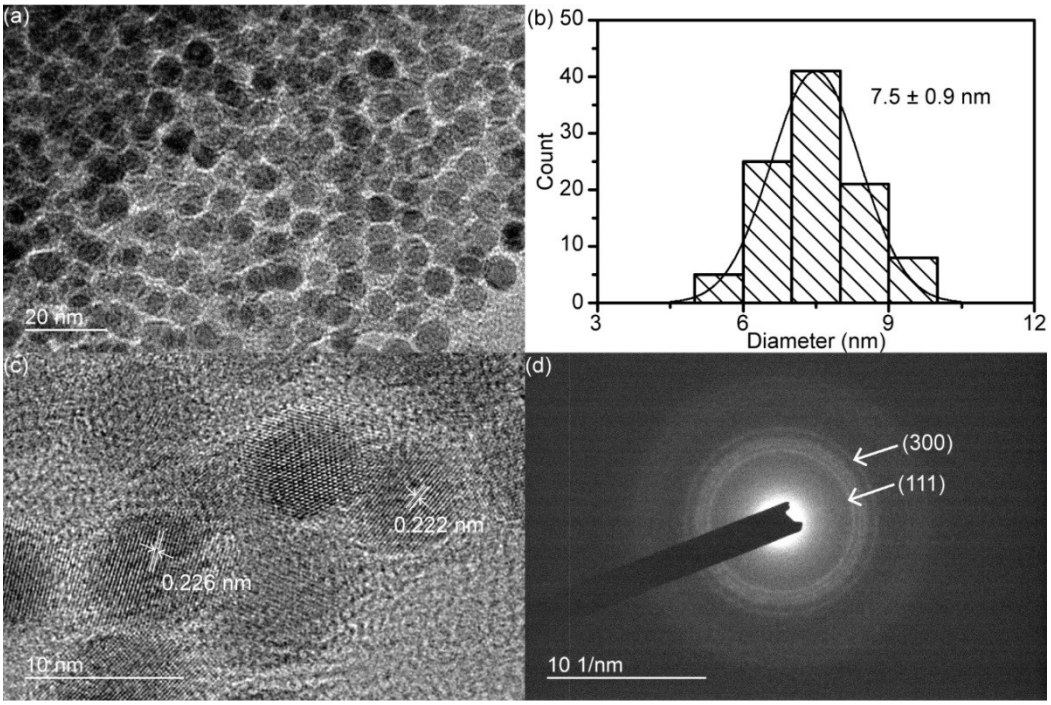

Figure S2. (a) TEM image, (b) and its size distribution, (c) high resolution TEM image, and (d) electron diffraction pattern of NiFeP nanoparticles.

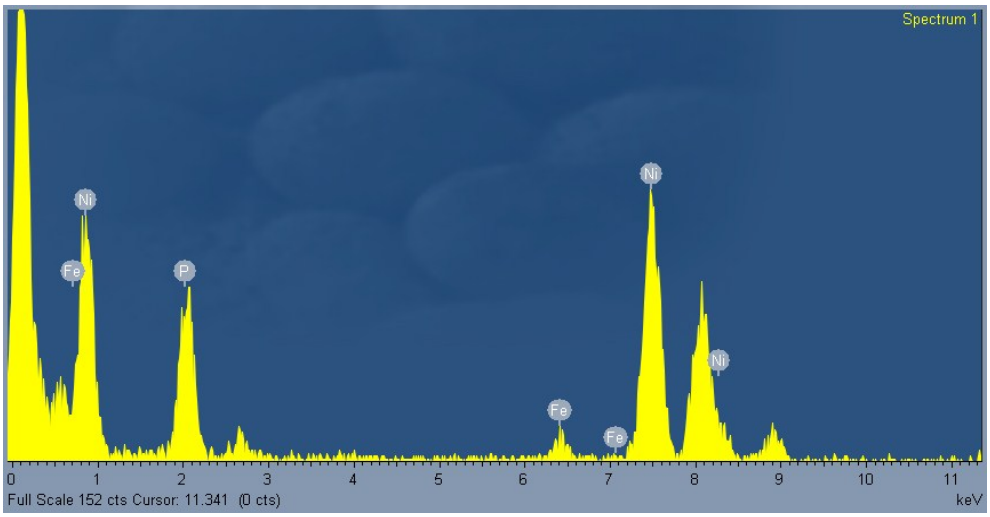

Figure S3. EDX spectrum of NiFeP nanoparticles.

The scope of metal doping is extended to other transition metal ions including cobalt, manganese, and molybdenum ions at high 1:1 doping as NiMP. As a result, other transition metal acetate is used instead of iron(II) acetate as a precursor in synthesis to prepare other transition metal-doped nickel phosphides (NiMP) nanoparticles. The corresponding XRD patterns (Figure S4), TEM images (Figure S5) and composition (Table S1) of NiMP nanoparticles all resemble closely to the Ni_2P reference (PDF#-65-1989, Figure S4) without much peak shift/distortion despite the large extent of transition metal incorporation.

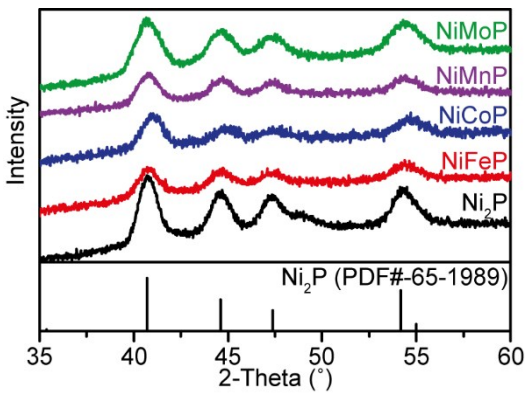

Figure S4. XRD patterns of Ni_2P and various NiMP nanoparticles.

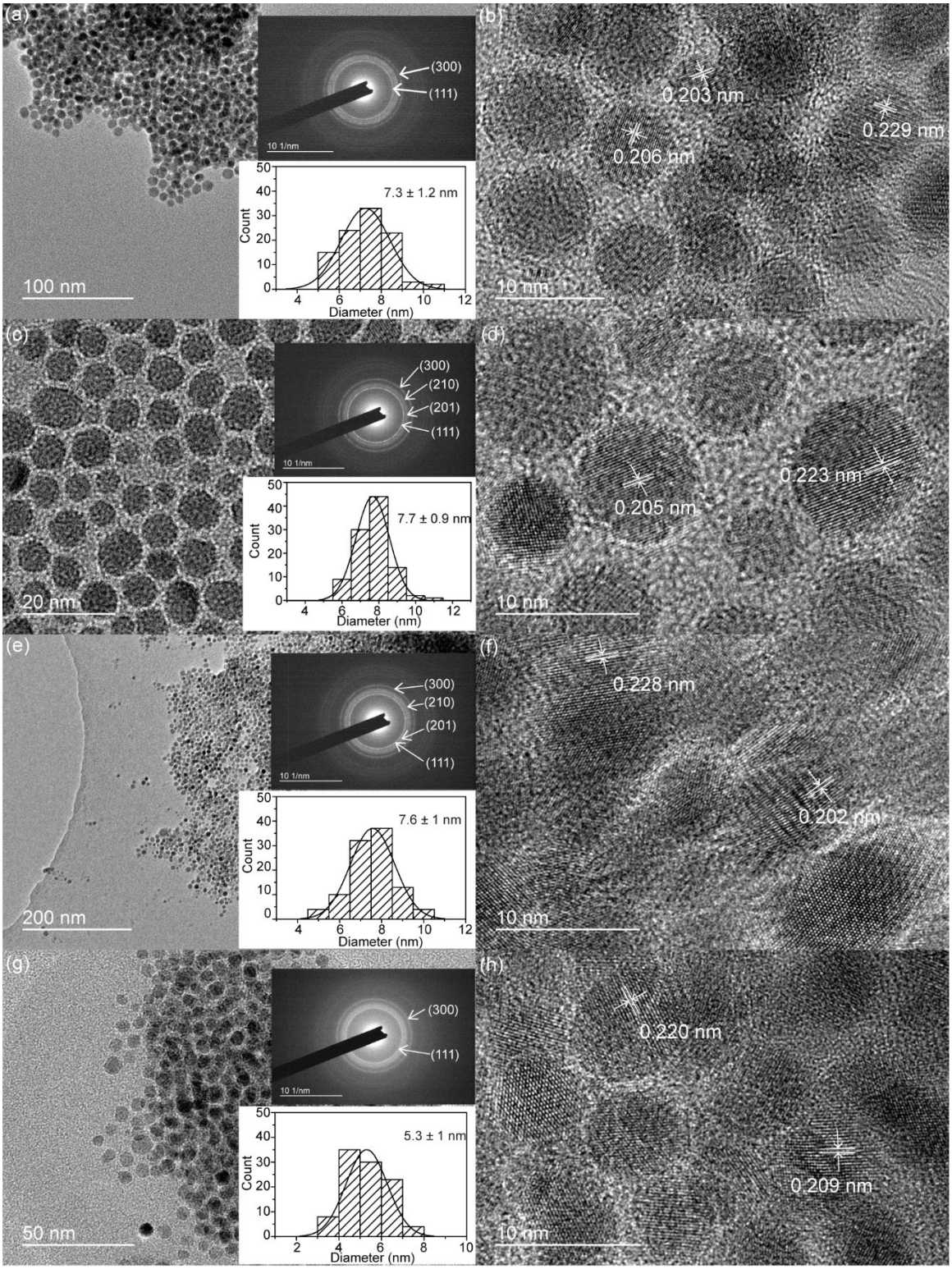

Figure S5. TEM and HR-TEM images with selected area electron diffraction pattern and size distribution in inset. (a and b) Ni_2P, (c and d) NiCoP, (e and f) NiMnP, (g and h) NiMoP nanoparticles showing same morphology and homogeneous doping with comparable lattice fringes observed.

Table S1a. Metal precursor loading for synthesis of pristine and metal-doped nickel phosphide nanoparticles.

	Metal precursor(s)
Ni_2P	$Ni(OAc)_2 \cdot 4H_2O$ (1 mmol)
NiFeP	$Ni(OAc)_2 \cdot 4H_2O$ (0.5 mmol) + $Fe(OAc)_2$ (0.5 mmol)
NiCoP	$Ni(OAc)_2 \cdot 4H_2O$ (0.5 mmol) + $Co(OAc)_2$ (0.5 mmol)
NiMnP	$Ni(OAc)_2 \cdot 4H_2O$ (0.5 mmol) + $Mn(OAc)_3 \cdot 2H_2O$ (0.5 mmol)
NiMoP	$Ni(OAc)_2 \cdot 4H_2O$ (0.5 mmol) + $[Mo(OAc)_2]_2$ (0.25 mmol)

Table S1b. Normalized elemental composition of pristine and metal-doped nickel phosphide nanoparticles by EDX

	Ni	M	P
Ni_2P	2	-	1
NiFeP	1	0.1	0.7
NiCoP	1	0.55	1.2
NiMnP	1	0.05	0.7
NiMoP	1.6	0.08	1

XPS spectra of NiFeP nanoparticle in Ni 2p and P 2p regions also have the peaks similar to typical nickel phosphides (Figure S6a and c).[3] Peaks at 853.0 eV correspond to nickel in nickel-phosphorus bond in Ni $2p_{3/2}$ level. The binding energy is close to zero-valent nickel (852.8 eV)[4] which indicates nickel in nickel-phosphorus bond only bear a small positive charge ($Ni^{\delta+}$).[5] The peaks at 856.1 and 861.5 eV are assigned to the oxidized nickel species (NiO) and its satellite peak in Ni $2p_{3/2}$ level, respectively. Similarly, the peaks at 869.9, 874.1, and 880.1 eV correspond to nickel in nickel-phosphorus bond, oxidized Ni species, and its satellite peak in the Ni $2p_{1/2}$ energy level. In XPS spectrum of P 2p region, the peak at 129.4 eV originates from the phosphorus in nickel-phosphorus bond, while the peak at 133.1 eV corresponds to the surface oxidized phosphorus species such as phosphate. The binding energy of phosphorus in phosphide slightly deviates from elemental phosphorus (130.2 eV) which shows phosphorus in nickel-phosphorus bond bears a small negative charge ($P^{\delta-}$).[6] In addition, the embedded peak at 130.4 eV can be assigned to the phosphorus in iron phosphide domain.[7] For Fe 2p XPS spectrum, the peaks at 711.8 and 713.5 eV correspond to the surface oxidized iron in iron oxide and phosphate in Fe $2p_{3/2}$ energy level, respectively, meanwhile the peaks at 723.5 and 727.9 eV are the counterpart peaks in Fe $2p_{1/2}$ energy level.[8] The peaks at 706.8 and 719.5 can be assigned to the iron in iron phosphide in Fe $2p_{3/2}$ and $2p_{1/2}$ energy level, respectively (Figure S6b).

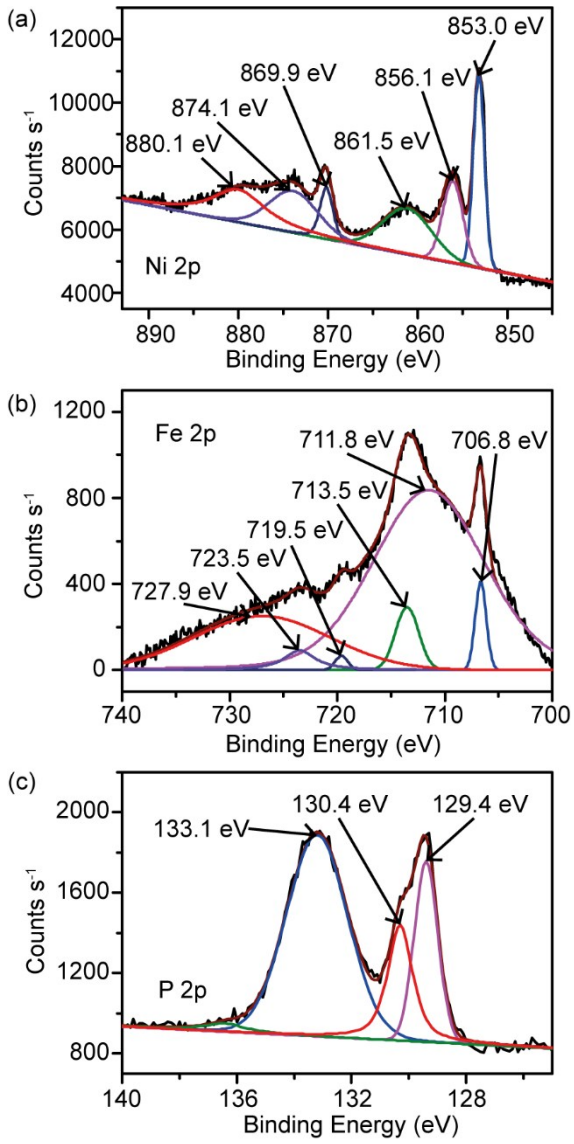

Figure S6. XPS spectra of NiFeP nanoparticle in (a) Ni 2p, (b) Fe 2p, and (c) P 2p.

NiP structure

According to the experimental XRD data *NiP* structure (stoichiometric and non-stiochiometric from 1:1 to 2:1) resembles to the wurtzite structure of ZnO. As a result, 3D lattice as the prototype host matrix to represent the NiP structure is attempted. The Ni is placed in the position of Zn site and the P is placed in the O site. After the geometrical lattice relaxation under the zero external hydrostatic pressure, the ground state structure of the *NiP* follows the symmetry group of *P63/mmc* with structural formula of Ni_2P_2. Figure S7

demonstrates the predicted crystal structure lattice arrangement for this *NiP* structure. The reciprocal path for the band structure calculations is from Γ (0, 0, 0) to the H (0, 0, ½). The total density of states (TDOSs) plot shows the strong *p-d* coupled orbital level across the Fermi level (E_F) by Ni-P hybridized bonding.

In the band structure of the BZ, it shows an isotropic metallic behavior indicating a good electronic conductor for charge transfer without barrier. The H point gives a gap up to about 5 eV, denoting the electronic transfer cannot be easily attributed to the path along the Ni-P bonding direction in the real space. There might be another possible mechanism e.g. Coulomb tunneling for charge transfer. Meanwhile, it also means the electronic transport in such conductor is mostly along the direction perpendicular to the plane (i.e. along z-axis) instead of transferring along the in-plane Ni-P bonding direction.

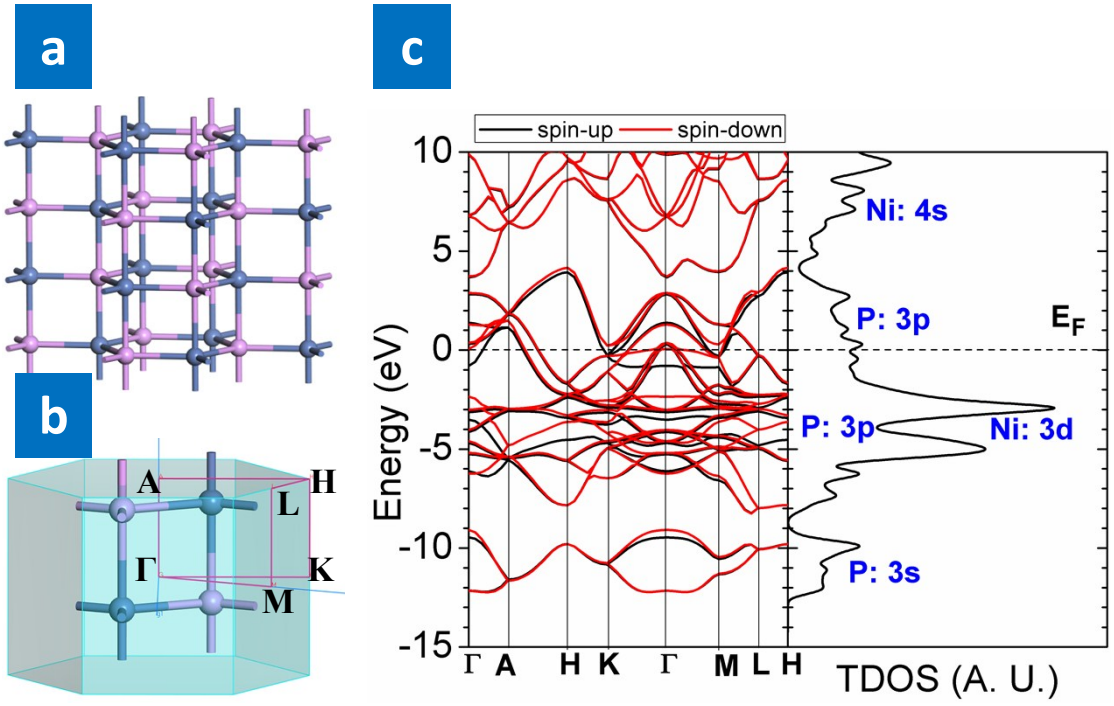

Figure S7. (a) The predicted Ni_2P_2 crystal structure. (b) The related unit cell lattice with reciprocal Brillouin Zone (BZ) presented. (c) The right panel is the electronic band structure and total density of states (TDOSs) along the path formed by the high symmetrical points in the BZ. (Ni=grey, and P=purple).

Metallic structure

Ultra-violet photoelectron spectroscopy (UPS) is carried out for NiFeP nanoparticle to determine the energy of valence band maximum against Fermi level (Figure S8). The energy difference between Fermi level (E_F) and valence band maximum (E_{VBM}) can be found from the interception on abscissa by extrapolating the right-side slope of the peak. The energy difference is estimated as -0.37 eV that implies a higher energy of valence band maximum (VBM) than Fermi level and confirms NiFeP nanoparticle possesses a metallic property as that of *NiP* structure.

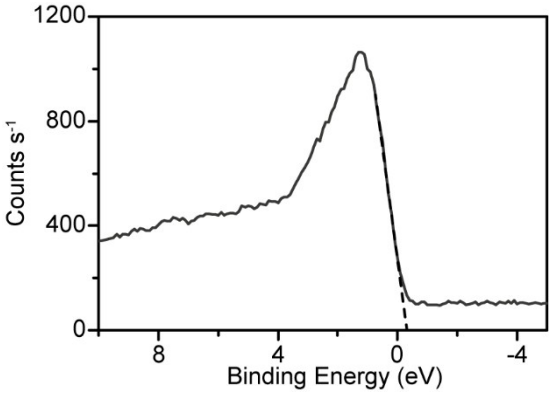

Figure S8. UPS spectrum of NiFeP nanoparticle.

EXAFS studies

Based on the structural analyses of NiFeP and Ni_2P nanoparticles, NiFeP nanoparticle is proved to be synthesized without a significant change in nickel phosphide crystal structure. However, it is difficult to determine the exact localized bonding environments of iron in the crystal lattice by the aforementioned characterizations. In order to have further information on the structure, the extended X-ray absorption fine structure (EXAFS) measurement is carried out. It measures the average coordination number of surface atoms and estimates bond lengths, and thus helps getting a better picture on the bonding environment and local structure of each element in NiFeP nanoparticle. The data for NiFeP nanoparticle were recorded and the fittings were carried out with satisfaction (Figure S10, Figure S11, and Table S3), which

depicted the hcp structure (Figure S7). The bond lengths of various combinations of elements are estimated, including nickel-phosphorus (Ni-P), nickel-nickel (Ni-Ni), iron-nickel (Fe-Ni), and iron-phosphorus (Fe-P) bonds. Ni-Ni and Ni-P bonds are 2.59 and 2.24 Å, respectively. Meanwhile, Fe-Ni and Fe-P bonds are 2.63 and 2.21 Å, respectively. The EXAFS data confirmed the existence of iron incorporation in nickel phosphide and iron is bonded to both nickel and phosphorus in the hcp crystal lattice as illustrated in Figure S7. The fitted data from EXAFS measurement of Ni_2P nanoparticle show the Ni-Ni and Ni-P bond lengths in Ni_2P nanoparticle are 2.59 and 2.25 Å, respectively (Figure S9 and Table S2). The bond lengths in iron-doped and pristine nickel phosphide nanoparticle are comparable which shows the incorporation of iron in nickel phosphide crystal lattice do not induce significant changes in bond strengths of existing Ni-Ni and Ni-P bonds. Typical coordination numbers in Ni-Ni and Ni-P for Ni_2P are 4 and 2, respectively, which are close to the fittings shown in Table S2, having coordination numbers for Ni-Ni and Ni-P as 3.3 and 2.9, respectively.[9] There is, however, a decrease in the coordination numbers when Fe is introduced into the crystal lattice. The coordination numbers for Ni-Ni and Ni-P in NiFeP nanoparticles are 2.5 and 2.3, respectively, whereas those for Fe-Ni and Fe-P are determined to be 3.6 and 3.7, respectively. The decreased coordination numbers of Ni-Ni and Ni-P indicate successful substitution of Ni with Fe. In addition, the change in coordination number does not reveal a perfect substitution since there is a degree of mismatch between the added coordination numbers of Ni-P and Fe-P in NiFeP nanoparticle and that of Ni-P in Ni_2P nanoparticle. But, the basic hcp structure is clearly maintained. From the above control experiments for NiFeP nanoparticle synthesis, it was confirmed that iron present in the reaction environment can be incorporated into nickel phosphide crystal lattice without making much significant effect on the morphology, crystal structure, and bonding environment of the resulting nanoparticles despite the large degree of Fe incorporation.

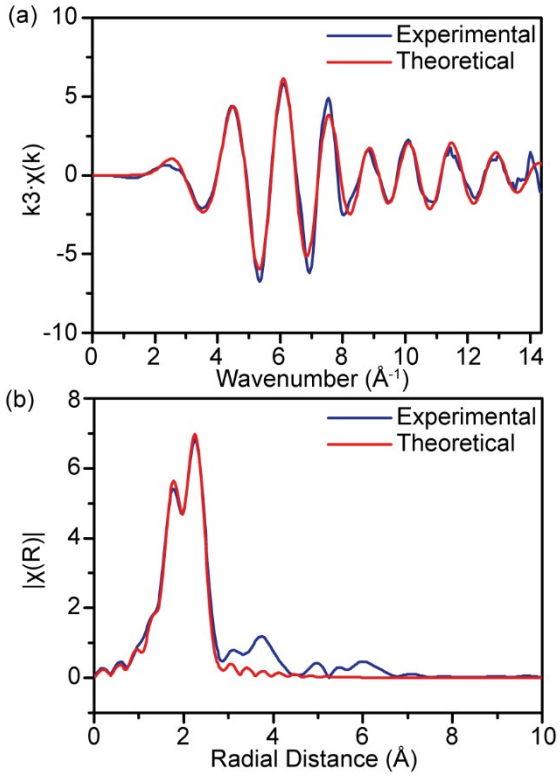

Figure S9. EXAFS plots of (a) $k^3 \cdot \chi$ of experimental and fitted data and (b) $k^3 \cdot \chi$ phase corrected Fourier transform of experimental and fitted data for Ni_2P nanoparticle with Ni K-edge transmission mode.

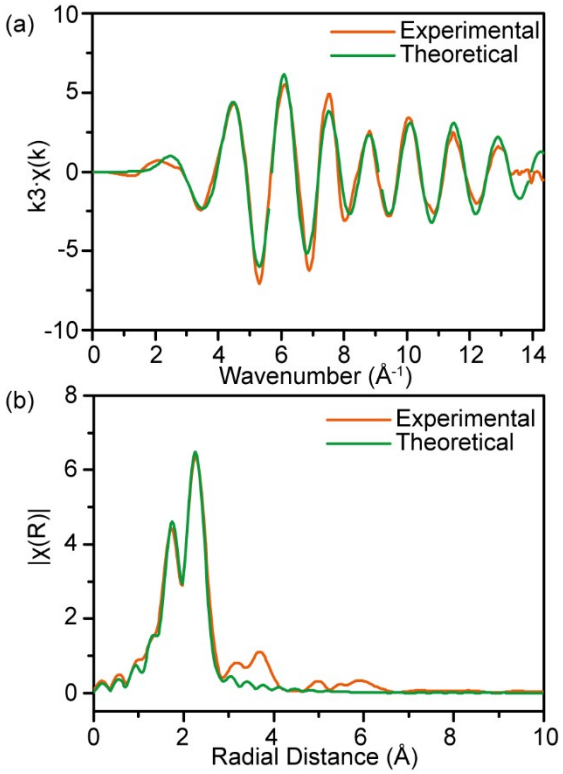

Figure S10. EXAFS plots of (a) $k^3 \cdot \chi$ of experimental and fitted data and (b) $k^3 \cdot \chi$ phase corrected Fourier transform of experimental and fitted data for NiFeP nanoparticle with Ni K-edge transmission mode.

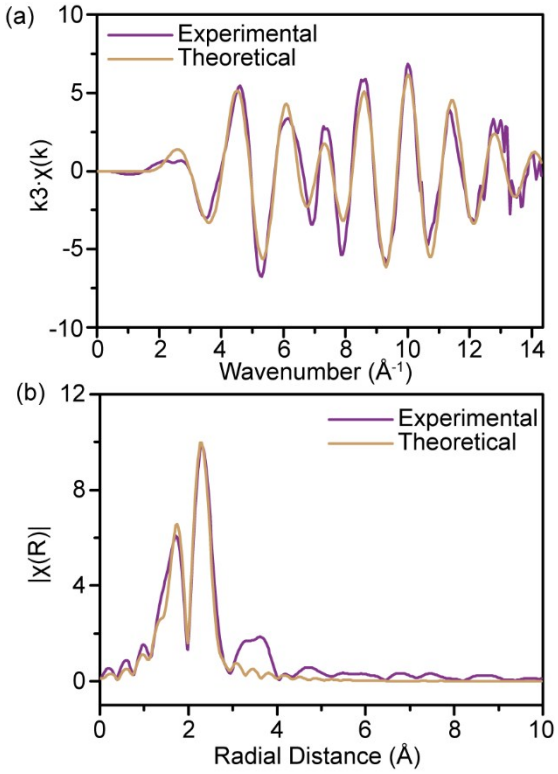

Figure S11. EXAFS plots of (a) $k^3 \cdot \chi$ experimental and fitted data and (b) $k^3 \cdot \chi$ phase corrected Fourier transform of experimental and fitted data for NiFeP nanoparticle with Fe K-edge transmission mode.

Table S2. EXAFS of Ni_2P nanoparticle.

Bond	Enot*	Coordination number	Ss	Bond length (Å)	R-factor
Ni-P	2.7	2.9(2)	0.008(1)	2.25(1)	0.6%
Ni-Ni		3.3(3)	0.008(1)	2.59(1)	

*Enot is the energy different of absorption energy in experimental value and calculated value.

Table S3 EXAFS of NiFeP nanoparticle.

Bond	Enot*	Coordination number	Ss	Bond length (Å)	R-factor
Ni-P	4.3	2.3(3)	0.008(2)	2.24(1)	1.3%
Ni-Ni		2.5(3)	0.006(1)	2.59(1)	
Fe-P	5.5	3.7(3)	0.007(1)	2.21(1)	2.0%
Fe-Ni		3.6(3)	0.005(1)	2.63(1)	

*Enot is the energy difference of absorption energy in experimental value and calculated value.

The above EXAFS experiments were carried out in B18 Diamond light source. Si(111) Double Crystal Monochromator (DCM) was used to scan the photon energy. The energy resolution ($\Delta E/E$) for the incident X-ray photons was estimated to be 2×10^{-4}. Transmission mode was adopted for Ni K-edge and Fe K-edge EXAFS measurements. To ascertain the reproducibility of the experimental data, at least two scan sets were collected and compared for each sample. The EXAFS data analysis was performed using IFEFFIT 1 with Horae packages 2 (Athena and Artemes). The spectra were calibrated with Ni and Fe metal foils as the references to avoid energy shifts of the samples. The amplitude reduction factors were obtained from EXAFS data analysis of the references, which were used as the fixed input parameters in the data fitting to allow the refinement in the coordination number of the absorption element. In this work, the first shell data analyses under the assumption of single scattering were performed with the errors estimated by R-factor.

Table S4. Summary of electrochemical parameters of pristine and various metal-doped nickel phosphide nanoparticles.

	Overpotential at 20 mA cm^{-2} (V)	Tafel slope (mV dec^{-1})
Ni_2P	0.39	58
NiFeP	0.33	39
NiCoP	0.41	52
NiMnP	0.55	63
NiMoP	0.43	86

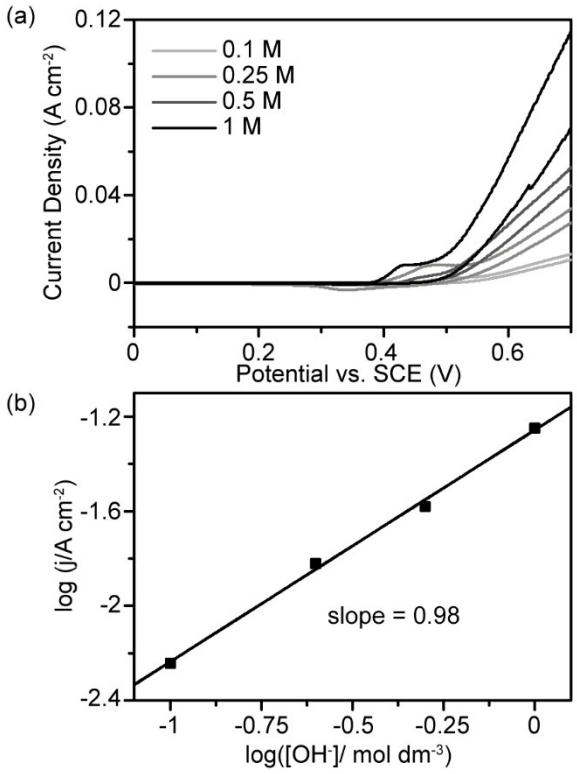

Figure S12. Cyclic voltammograms of NiFeP nanoparticle in KOH solution with different concentrations and (b) relationship between current density at 0.6 V vs. SCE and concentration of hydroxide ion.

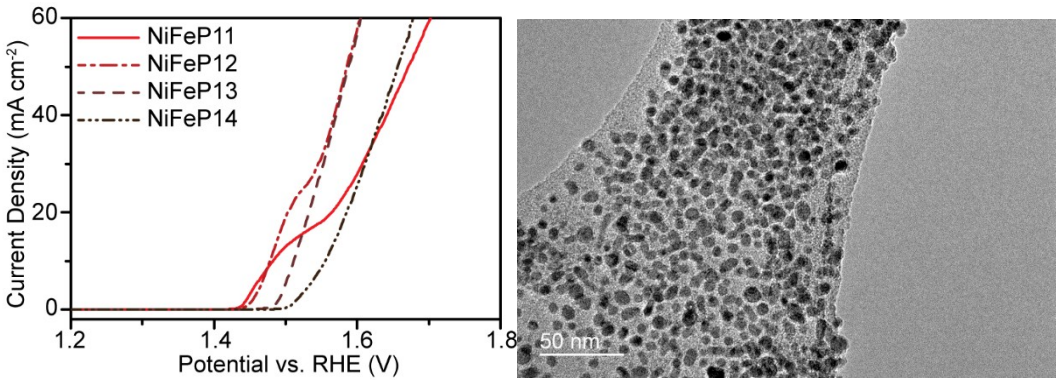

Figure S13. (a) The overpotentials of NiFeP at different Ni: Fe precursor ratios (from 1:1; 1:2; 1:3 and 1:4) for electrochemical OER are shown. (b) A typical TEM image of NiFeP12 sample showing a degree of inhomogeneity in elemental distributions of different contrasts.

NiFeP at different Ni: Fe precursor ratios for electrochemical OER have also been evaluated (Fig. S13a). It is apparent that the order of activity (inversed order of overpotential) is increased upon increasing iron content and reached the highest activity for NiFeP12 nanoparticle. Further increase in Fe loading (NiFeP13 and NiFeP14) leads to a decrease in activity. This volcano activity to Fe content is consistent with the anticipated synergetic effect between Fe and Ni and their surface oxyhydroxides as discussed in Fig. 3 and Fig. 4a of the main manuscript. However, we are cautious a degree of inhomogeneity in elemental distributions (NiFeP12 sample) was seen by the TEM image (Fig. S13b), which may lead to deviation

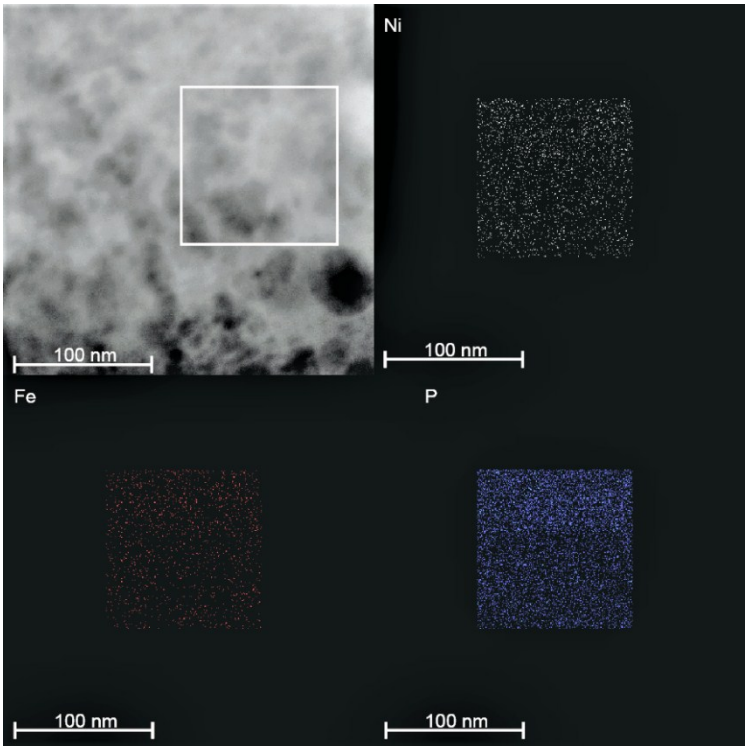

Figure S14 The EDX mapping of NiFeP nanoparticles after the long-term stability test showing Ni (white dots), Fe (red dots) and P (blue dots) are still fairly evenly distributed.
EDX mapping of post mortem NiFeP nanoparticles was obtained and is shown in Figure S14. The three elements (Ni, Fe, and P) appear to be evenly distributed.

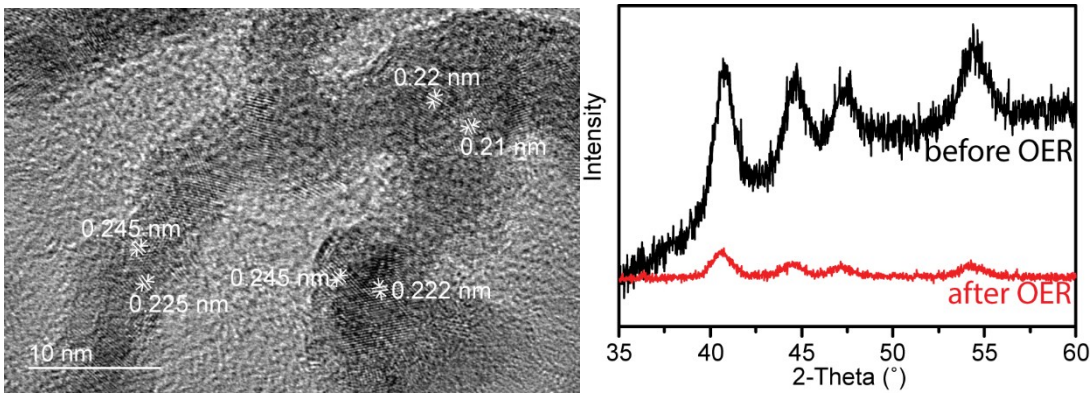

Figure S15 (a) The post-mortem HR-TEM analysis of NiFeP nanoparticles after the long-term stability test, which shows a deformation in particle shape (sintering). The lattice fringe separations indicate the formation of a small degree of nickel oxide (0.21 and 0.24 nm) in the major Ni(Fe)P phase (0.22 nm); (b) The XRD shows no significant difference in the Ni(Fe)P phase and there is no detection of the oxide indicating that it is not sensitive to detect the thin surface oxide layer using the XRD solely.

HR-TEM image of post-OER catalyst (Fig. S15a) was obtained and the fringe separations were also measured. It appeared that there is a deformation in particle shape (sintering) against the original finely-divided monodispersed nanoparticles. In addition, the fringe separations indicate the formation of a small degree of nickel oxide (0.21 and 0.24 nm) in the major Ni(Fe)P phase (0.22 nm). However, XRD (Fig. S15b) shows no significant difference in the Ni(Fe)P phase and there is no detection of the oxide indicating that it is not sensitive to detect the thin surface oxide layer using the XRD.

Thus, this type of materials is active for OER with good stability. It is also found that the same materials show to be a very good electrocatalyst for HER with satisfactory stability. For example, NiMoP gives a very low over-potential of 0.34 V in alkaline medium. In this paper, we intend to report the OER performance of different NiMP nanoparticles. We will report the HER performance in a separate paper.

Reference

1 F. Lyu, Y. Bai, Q. Wang, L. Wang, X. Zhang, Y. Yin, Dalton Trans. 2017, ***46***, 10545.

2 M. E. G. Lyons, M. P. Brandon, Int. J. Electrochem. Sci. 2008, ***3***, 1386.

3. Y. Pan, Y. Liu, J. Zhao, K. Yang, J. Liang, D. Liu, W. Hu, D. Liu, Y. Liu, C. Liu, J. Mater. Chem. A 2015, ***3***, 1656.

4. A. B. Mandale, S. Badrinarayanan, S. K. Date, A. P. B. Sinha, J. Electron Spectrosc. Relat. Phenom. 1984, ***33***, 61.

5. Z. Huang, Z. Chen, Z. Chen, C. Lv, H. Meng, C. Zhang, ACS Nano 2014, ***8***, 8121.

6. a) J. Li, Y. Chai, B. Liu, Y. Wu, X. Li, Z. Tang, Y. Liu, C. Liu, Appl. Catal., A 2014, ***469***, 434; b) Y. Zhao, Y. Zhao, H. Feng, J. Shen, J. Mater. Chem. 2011, ***21***, 8137.

7. C. E. Myers, H. F. Franzen, J. W. Anderegg, Inorg. Chem. 1985, ***24***, 1822.

8. a) Y. Yan, B. Y. Xia, X. Ge, Z. Liu, A. Fisher, X. Wang, Chem. - Eur. J. 2015, ***21***, 18062;

b) J. Masud, S. Umapathi, N. Ashokaan, M. Nath, J. Mater. Chem. A 2016, ***4***, 9750.

9. H. R. Seo, K-S. Cho, S-H. Kim, Y-K. Lee, J. Korean Phys. Soc. 2010, ***56***, 2083-2087.